Sensitive chemoselectivity of cellulose nanocrystal films

Wenna Ge
Dalian University of Technology
Zhixin Feng
Dalian University of Technology
Fusheng Zhang
Dalian Institute of Chemical Physics
Xiangge Bai
Dalian University of Technology
Shile Feng
Dalian University of Technology
Yahua Liu (yahualiu@dlut.edu.cn)
Dalian University of Technology https://orcid.org/0000-0003-4671-698X

Research Article

Keywords: Cellulose nanocrystals, Hydrolysis, Chemoselectivity, Nematic structure, Mesoporous carbon films

Posted Date: November 23rd, 2021

DOI: https://doi.org/10.21203/rs.3.rs-1024022/v1

Version of Record: A version of this preprint was published at Cellulose on April 4th, 2022. See the published version at https://doi.org/10.1007/s10570-022-04543-4.

Abstract

Cellulose nanocrystals (CNCs) self-assembled into a chiral nematic structure film is an advanced platform for the fabrication of fascinating sensing, photonic and chiral nematic materials. Despite extensive progress in the functions of CNCs, their chemoselectivity has rarely been reported. Here, we exploit a brand-new perspective of CNCs in chemoselectivity, which shows sensitive selectivity even between isomers of monosaccharides and disaccharide by generating discernible crystal patterns. This sensitive selectivity of glucose homologs is attributed to the selective interaction of carbohydrate–carbohydrate, which enables the tune of the photonic properties and chiral mesoporous structures. Moreover, based on the chemoselectivity, chiral mesoporous structures with tunable specific surface areas are assembled from CNC suspensions and glucose homologs. We envision that the sensitive chemoselectivity of CNC films could provide insights into the recognition of carbohydrates and the preparation of mesoporous carbon in numerous practical applications.

1. Introduction

Cellulose nanocrystals (CNCs) are biodegradable and sustainable polymers that could be hydrolyzed and extracted from cotton (Atalla et al. 1984; Lu et al. 2010; Saito et al. 2006), tree pulp (Claro et al. 2018; Lima et al. 2004) and bacteria (Arserim-Ucar et al. 2021; Dugan et al. 2013). Due to the chiral nematic phase (Gray et al. 2020; Zhang et al. 2020), high surface area (Chen et al. 2021; Elazzouzi-Hafraoui et al. 2008) and eco-friendly nature (Zhang et al. 2020; Sunasee et al. 2016), CNCs have been widely used in medical devices (Du et al. 2019; Ke et al. 2021; Palaganas et al. 2017), food packagings (Assis et al. 2021; Nascimento et al. 2018) and photonic materials (Lagerwall et al. 2014). Recent years have witnessed an increasing interest in introducing various foreign components into the CNC platform to control its optical response and chiral nematic structure (Bardet et al. 2015; Eremeeva et al. 2020; Querejeta-Fernandez et al. 2014; Roy et al. 2009; Tang et al. 2017; Xiong et al. 2020; Zhang et al. 2020). For instance, electric field has been applied to control the iridescence properties of CNCs at the micro-scale (Frka-Petesic et al. 2017; Manda et al. 2020). Magnet field, as a powerful and versatile tool, has also been used to control the CNC orientation and switch the structural colors in a programmed manner (Frka-Petesic et al. 2017). Besides, Qing et al. (2019) reported the chemoselectivity of pristine CNC film to saccharides, along with the color variation through the carbohydrate–carbohydrate interactions. However, there is still scarce study of the chemoselectivity of cellulose in isomers of glucose homologs, which is a powerful approach to recognize glucose homologs and prepare mesoporous carbon films.

In this work, we synthesize and screen out CNC precursors with excellent self-assembly capabilities by sulfuric acid hydrolysis through the control of hydrolysis temperature and time. The available yields of crystalline cellulose can reach more than 74wt% and the surface sulfur content can reach 0.95wt%. The resulting CNC suspension can be dried into a chiral nematic blue film by evaporation-induced self-assembly technique (Kang et al. 2013; Revol et al. 1998; Roman et al. 2005). The fabricated CNC film establishes sensitive selectivity between not only monosaccharides or disaccharide, but also their isomers, by forming distinct pattern morphologies in the crystalline process. We show that the crystal

morphologies are determined by the carbohydrate–carbohydrate interactions. Furthermore, we take the spatial carbohydrate–carbohydrate interactions to regulate the chiral nematic structure and fabricate mesoporous carbon films with a specific surface area ranging from 700 to 1350 m^2/g. We believe that the sensitive chemoselectivity and the tune of chiral mesoporous carbon films of CNC film can contribute to the development of sugar-based sensors (Egawa et al. 2011; Suresha et al. 2008), chiral recognition (Chen et al. 2021; Li et al. 2021) and large-scale chiral structures (Lin et al. 2021; Tan et al. 2021).

2. Experimental Section

2.1 Fabrication of film

Materials. Cotton was bought from a market (Dalian, China) without any further processing. The analytical grade chemical sulfuric acid (H_2SO_4, 98%), d-glucose, d-galactose, d-lactose, and d-sucrose were purchased through standard suppliers. Polystyrene Petri dishes with a diameter of 5 cm were supplied by Guangzhou Jet Bio-Filtration Co., Ltd.

Preparation and purification of CNC suspensions. The CNCs were prepared by acidic hydrolysis at a temperature ranging from 35, 45 to 65 ℃ and the time ranging from 60, 90, 120 to 150 mins. The acid hydrolysis process was conducted at a ratio of 1:15 g/mL (solid cotton to sulfuric acid). The sulfuric acid solution (64wt%) was heated to a certain temperature in advance. After the temperature was constant, a certain proportion of the solid cotton was added to the solution and stirred vigorously. The hydrolysis reaction was conducted with a large amount of ultrapure water and the solution was allowed to stand for a night. The supernatant was poured out at any time, which was repeated several times until it was not layered. After that, the suspension without stratification was centrifuged at 6000 rpm/min for 10 minutes. The dispersion and centrifugation processes were repeated at least three times. At last, it was dialyzed using deionized water through a cellulose ester dialysis membrane (12,000–14,000 molecular weight wiped off) until constant pH was reached (typically over 4-5 days). The process for cellulose hydrolysis with sulfuric acid was shown in Fig. S1.

The sample sulfur content hydrolyzed by sulfuric acid. The sulfur contents of the suspension was often cited to evaluate the stability and charge content of the samples (Abitbol et al. 2013). After the removal of excess acid, the suspension of CNC dispersion (2.0wt%, 5 g) in presence of NaCl solution (1 mM, 75 g) is titrated with NaOH (50 mM). NaCl gave a certain ionic strength to limit repulsions in mixture due to the charged groups presented at the surface of CNCs. The sulfur content in solution could be quantified (Fig. S2). Because of charge repulsion, CNCs were dispersed in water and organized into a chiral nematic lyotropic liquid crystalline phase, which could be captured in a solid film when the dispersing medium was slowly evaporated.

Preparation of the mesoporous carbon films. Using the chiral phase of cellulose, the mesoporous silicon template (tetraethoxysilane, 200 μl) was introduced into the cellulose suspension (3wt%, 5 ml). The same

proportion of different types of glucose homologs (28wt%) was added. The mixed solution was stirred at room temperature for 1 hour, and then placed in a petri dish and dried for 24 hours to obtain a mixed film.

Carbonization and de-templating of the nanocomposite cellulose film. The mixed film was put into the tube furnace filled with nitrogen with a heating rate of 2 ℃/min to 100 ℃ and kept for 2 hours. Then the temperature was raised to 600 ℃ at the same heating rate, and maintained for 6 hours. After that, the furnace was slowly cooling down to room temperature, and a carbonized carbon/silica composite film was obtained. Finally, the black film was put in a 2 M NaOH solution (200 ml), and stored at 90 ℃ for 4 h to remove SiO_2.

2.2 Surface characterization

Transmission electron microscopy (TEM). The TEM sample was prepared by putting dilute dispersion (~0.01wt%) of cellulosic suspension onto carbon-coated grids. 10 uL CNC suspension was dispersed on a glow-discharged carbon-coated copper network (300-mesh copper, Ted Pella Inc) and filter paper was used to remove excess liquid and then characterized on a JEOL JEM-2100 (HR) with an accelerating voltage of 200 kV with a LaB6 filament.

Scanning electron microscopy (SEM) and polarized optical microscopy (POM). The surface morphology was characterized using a Carl Zeiss electron microscope with ORION NanoFab. The sample was fractured after being frozen by liquid nitrogen and the section was collected. POM images were captured using an Olympus BX53 optical microscope.

Atomic force microscopy (AFM). An appropriate concentration of CNC dispersion (~ 0.005wt%) was transferred to the mica plate and dried at room temperature. NanoWizard ULTRA Speed JPK in QITM mode was used to image the samples. To obtain a good characterization, a uniformly dispersed sample at a low concentration was prepared. Figure 1a shows the AFM images of samples with hydrolysis time 60 mins, 90 mins, 120 mins and 150 mins, respectively.

3. Results And Discussion

The hydrolysis time and temperature were first screened out for extracting cellulosic suspension from cotton. Here, the hydrolysis time and temperature were changed from 60 to 150 mins and 35 to 55 ℃, respectively. During the hydrolysis reaction, the amorphous regions of cellulose were selectively hydrolyzed, leaving the crystalline regions known as CNCs with spindle-shaped nanoparticles (Fig. S3). Also, a protonated sulfate group ($–OSO_3$) was introduced into the surface of the CNC nanoparticles, which was detected by a conductivity titration method. The sulfur content and charge density under different reaction conditions were shown in Fig. S4. With the reaction temperature increased, the sulfur content (wt%) increased first and then decreased due to the excessive hydrolysis of the CNC nanoparticles. Meanwhile, the sulfur content increased with the reaction time at the same temperature (Fig. S4a). Note that, the charge density was kept almost constant (Fig. S4b).

Based on the charge repulsion induced by $-OSO_3$, a chiral CNC film was obtained via a simple and environmental evaporation-induced self-assembly method. It was shown that the aspect ratio of obtained CNCs decreased as the hydrolysis time increased as shown in Fig. 1a, and the optimal hydrolysis temperature 45 ℃ was screened out to obtain the largest CNC yield (~74.1wt%) at this condition (Fig. 1b). Further optical photos showed that the structural color of CNC films could be controlled from colorless to reddish with hydrolysis time varying from 60 to 150 mins (Fig. 1c). Moreover, we found that distinct fingerprint in macro-scale was generated on each CNC film, as shown in Fig. 1d. Figure 1e showed the SEM images of the micro-scale structures of CNC films, which manifested different pitches (P) ranging from 238 nm, 309 nm, 370 nm to 394 nm, respectively, with the increase of hydrolysis time. To explore the relationship between micro-structures and structural colors, we detected the reflection wavelength (λ) of the films by a spectrophotometer (Fig. 1f). It could be seen that the hydrolysis time resulted in a red-shift of the reflection band. In addition, the reflected wavelength was positive to the pitch value P, which was consistent with De Vries equation (Devries et al. 1951): $\lambda_{max} = n_{avg}P$. Here, n_{avg} was the average refractive index. We believe that the unique chiral nematic structures will provide a new insight in chemoselectivity.

To explore the chemoselectivity of the CNC film, we examined the crystalline morphologies of glucose homologs including monosaccharides, disaccharide and their isomers, whose molecular formulas were shown in Fig. 2a. During the experiment, we dripped the glucose homologs solution (200 mmol/mL, 200 μl) on the CNC film drop by drop. Then, the glucose homologs crystallized on the target surface, as shown in the schematic in Fig. 2b. Obviously, the crystalline morphologies of various glucose homologs were distinct among not only monosaccharides and disaccharide, but also their isomers, though there were only differences in the spatial isomerization of -OH in the molecular structure (Fig. 2a).

In the crystallization process, the glucose precipitated and spread gradually to generate glittering and translucent snowflake-like structures (Fig. 2c and Fig. S5). However, the crystallization process of galactose (the isomer of glucose) was obviously different, forming a flower-like structure (Figs. 2c and S6). Similarly, for lactose and its isomer, the crystalline morphologies were also distinct, which exhibited structures of forked branches and patches of feathers, respectively (Fig. 2c). Moreover, we observed similar crystalline morphologies of glucose homologs on glass plates, as shown in Fig. 2d. The above discrepancy shows that the CNC films establish sensitive chemoselectivity of not only monosaccharides and disaccharide, but also their isomers by forming distinct pattern morphologies in crystalline process. This sensitive selectivity is due to the carbohydrate–carbohydrate interactions between glucose homologs and CNC films, rather than the crystallization differences of glucose homologs themselves.

Note that, the carbohydrate–carbohydrate interactions between carbohydrates and sulfonated polysaccharide have been reported before (Bavireddi et al. 2013; Ji et al. 2019; Sletmoen et al. 2018), which can be detected by colloidal probe microscopy (Lorenz et al. 2012; Witt et al. 2016). Here, the carbohydrate–carbohydrate interactions between CNC film and glucose homologs are shown in Fig. 3a. Different crystalline morphologies are attributed to the hydrogen bonds with different conformations, formed by the isomerization of hydroxyl groups in isomers of glucose homologs. Moreover, the selective

interaction between various glucose homologs and CNC films can be used to regulate the porous structure of carbon (Gan et al. 2021; Gao et al. 2021; Wang et al. 2021). As carbohydrate–carbohydrate interactions between glucose homologs are weak, the influence of glucose homologs to the micro structure of CNCs film would be small. When glucose homologs are mixed into CNCs, the pitch value *P* could be disturbed due to the carbohydrate–carbohydrate interaction as shown in Fig. 3b. After further carbonization and de-templating process, a carbonized material with long range ordered mesopores is obtained assembled from CNCs and glucose homologs (CNCs/glucose) film, and a schematic is shown in Fig. 3c. Moreover, the pitch value *P* of the carbonized films is influenced by the types of glucose homologs, which are 327 nm, 384 nm, 346 nm and 365 nm, respectively, in contrast to the *P* of original CNC films (370 nm), as shown in Fig. 3d. This further verifies the distinction of selective interactions between various glucose homologs and CNCs.

Not only the chiral structure of carbonized films, but also the pore structural feature of carbonized materials including specific surface area, pore volume and diameter, determine their applications. Following is an example of the mesopore carbonized material assembled from the CNCs and sucrose (CNCs/sucrose). The carbonized CNCs/sucrose material has inherited the chiral structure as well as the functions of cellulose, as evidenced in the transmission electron microscopy (Fig. 4a). According to the nitrogen adsorption and desorption isotherm of carbonized CNCs/sucrose material which exists a hysteresis loop, the adsorption isotherm could be labeled as Type V (Kazmierczak-Razna et al. 2017), which provides insight into the pore type of the material (Deng et al. 2020). Besides, we apply the Barret–Joyner–Halenda model (Fig. 4c) to calculate the peak pore diameter of CNCs/sucrose material (~ 3.3 nm), which is an idea carrier for catalyst.

Further, the influence of glucose homologs on specific surface area, pore volume and diameter was investigated. For CNC carbon films without glucose homologs, as shown in Fig. 4d and Table S1, the specific surface area, pore volume and diameter are 705 m^2/g, 1.02 cm^3/g and 3.7 nm, respectively. However, after monosaccharides or disaccharides are added into cellulose solution, the surface area of CNC carbon film is nearly doubled (Fig. 4d), while the pore volume and pore diameter are both slightly reduced (Table S1). This is attributed to the increased mesoporous of CNC films when added with glucose homologs compared to the original ones. Therefore, we can fabricate the mesoporous carbon films with tunable specific surface area assembled from CNC suspensions and various glucose homologs.

4. Conclusions

In summary, we prepared CNC precursors by sulfuric acid hydrolysis through the control of hydrolysis conditions, whose yield, sulfur content and reflectance spectra could be controlled with different preparation conditions. The CNC films show sensitive chemoselectivity to glucose homologs including monosaccharides, disaccharide and their isomers, which is attributed to the selective carbohydrate–carbohydrate interactions between CNC films and glucose homologs. Besides, this distinct interactions can be utilized to fabricate mesoporous carbon films with tunable specific surface area assembled from

CNC suspensions and glucose homologs. We expect that the sensitive chemoselectivity of CNCs opens up a new avenue for recognizing carbohydrates and fabricating mesoporous carbon films, which shows great potential in the fabrication of sugar-based sensors, electrode materials nanodevices, energy storage devices, etc.

Declarations

Acknowledgments

We are grateful for the support from National Natural Science Foundation of China (52075071, 51605073, 52005075), the Fundamental Research Funds for the Central Universities (DUT18RC(3)048, DUT19RC(3)055), Liao Ning Revitalization Talents Program (XLYC1807092) and Opening Project of the Key Laboratory of Bionic Engineering (Ministry of Education), Jilin University (KF20200002). Y. L. and S. F. acknowledge support from the Star Ocean Outstanding Talents Program.

References

Abitbol T, Kloser E, Gray DG (2013) Estimation of the surface sulfur content of cellulose nanocrystals prepared by sulfuric acid hydrolysis. Cellulose 20: 785-794. https://doi.org/10.1007/s10570-013-9871-0

Arserim-Ucar DK, Korel F, Liu LS, Yam KL (2021) Characterization of bacterial cellulose nanocrystals: effect of acid treatments and neutralization. Food Chem 336:127597. https://doi.org/10.1016/j.foodchem.2020.127597

Assis RQ, Pagno CH, Stoll L, Rios PD, Rios AD, Olivera FC (2021) Active food packaging of cellulose acetate: Storage stability, protective effect on oxidation of riboflavin and release in food simulants. Food Chem 349:129140. https://doi.org/10.1016/j.foodchem.2021.129140

Atalla RH, Vanderhart DL (1984) Native cellulose: a composite of two distinct crystalline forms. Science 223:283-285. https://doi.org/10.1126/science.223.4633.283

Bavireddi H, Bharate P, Kikkeri R (2013) Probing carbohydrate-carbohydrate interactions by photoswitchable supramolecular glycoclusters. Chem Comm 49:3988-3990. https://doi.org/10.1039/c3cc41025k

Bardet R, Belgacem N, Bras J (2015) Flexibility and color monitoring of cellulose nanocrystal iridescent solid films using anionic or neutral polymers. ACS Appl Mater Interfaces 7:4010-4018. https://doi.org/10.1021/am506786t

Chen W, Jiang JZ, Qiu GS, Tang S, Bai ZW (2021) The interactions between chiral analytes and chitosan-based chiral stationary phases during enantioseparation. J Chromatogr A 1650:462259. https://doi.org/10.1016/j.chroma.2021.462259

Chen WX, Chen B, Lv RX, Wu ML, Zhou J, Lu BL, Huang B, Lu QL, Tang LR (2021) Fabrication of quartz crystal microbalance humidity sensors based on super-hydrophilic cellulose nanocrystals. Cellulose 28:3409-3421. https://doi.org/10.1007/s10570-021-03777-y

Claro PIC, Correa AC, De Campos A, Rodrigues VB, Luchesi BR, Silva LE, Mattoso LHC, Marconcini JM (2018) Curaua and eucalyptus nanofibers films by continuous casting: Mechanical and thermal properties. Carbohydr Polym 181:1093-1101. https://doi.org/10.1016/j.carbpol.2017.11.037

Deng C, Zhu M (2020) New type nitrogen-doped carbon material applied to deep adsorption desulfurization. Energy Fuels 34:9320-9327. https://doi.org/10.1021/acs.energyfuels.0c00854

Devries H (1951) Rotatory power and other optical properties of certain liquid crystals. Acta Crystallogr 4:219-226. https://doi.org/10.1107/S0365110X51000751

Du HS, Liu WM, Zhang ML, Si CL, Zhang XY, Li B (2019) Cellulose nanocrystals and cellulose nanofibrils based hydrogels for biomedical applications. Carbohydr Polym 209:130-144. https://doi.org/10.1016/j.carbpol.2019.01.020

Dugan JM, Gough JE, Eichhorn SJ (2013) Bacterial cellulose scaffolds and cellulose nanowhiskers for tissue engineering. Nanomedicine 8:287-298. https://doi.org/10.2217/nnm.12.211

Egawa Y, Seki T, Takahashi S, Anzai J (2011) Electrochemical and optical sugar sensors based on phenylboronic acid and its derivatives. Mater Sci Eng C 31:1257-1264. https://doi.org/10.1016/j.msec.2011.05.007

Elazzouzi-Hafraoui S, Nishiyama Y, Putaux JL, Heux L, Dubreuil F, Rochas C (2008) The shape and size distribution of crystalline nanoparticles prepared by acid hydrolysis of native cellulose. Biomacromolecules 9:57-65. https://doi.org/10.1021/bm700769p

Eremeeva E, Sergeeva E, Neterebskaia V, Morozova S, Kolchanov D, Morozov M, Chernyshov I, Milichko V, Vinogradov A (2020) Printing of colorful cellulose nanocrystalline patterns visible in linearly polarized light. ACS Appl Mater Interfaces 12:45145-45154. https://doi.org/10.1021/acsami.0c11846

Frka-Petesic B, Guidetti G, Kamita G, Vignolini S (2017) Controlling the photonic properties of cholesteric cellulose nanocrystal films with magnets. Adv Mater 29:1701469. https://doi.org/10.1002/adma.201701469

Frka-Petesic B, Radavidson H, Jean B, Heux L (2017) Dynamically controlled iridescence of cholesteric cellulose nanocrystal suspensions using electric fields. Adv Mater 29:1606208. https://doi.org/10.1002/adma.201606208

Gan FL, Cheng BW, Jin ZH, Dai ZD, Wang BD, Yang L, Jiang X (2021) Hierarchical porous biochar from plant-based biomass through selectively removing lignin carbon from biochar for enhanced removal of toluene. Chemosphere 279:130514. https://doi.org/10.1016/j.chemosphere.2021.130514

Gao Y, He D, Wu L, Wang ZP, Yao YC, Huang ZH, Yang H, Wang MX (2021) Porous and ultrafine nitrogen-doped carbon nanofibers from bacterial cellulose with superior adsorption capacity for adsorption removal of low-concentration 4-chlorophenol. Chem Eng J 420:127411. https://doi.org/10.1016/j.cej.2020.127411

Gray DG (2020) Cellulose nanocrystal research; A personal perspective. Carbohydr Polym 250:116888. https://doi.org/10.1016/j.carbpol.2020.116888

Ji YM, Liu GJ, Li CY, Liu YC, Hou M, Xing GW (2019) Water-soluble glucosamine-coated AIE-active fluorescent organic nanoparticles: design, synthesis and assembly for specific detection of heparin based on carbohydrate-carbohydrate interactions. Chem Asian J 14:3295-3300. https://doi.org/10.1002/asia.201901153

Jian MQ, Zhang YY, Liu ZF (2020) Natural biopolymers for flexible sensing and energy devices. Chinese J Polym Sci 38:459-490. https://doi.org/10.1007/s10118-020-2379-9

Kang H, Liu R, Yong H (2013) Cellulose derivatives and graft copolymers as blocks for functional materials. Polym Int 62:338-344. https://doi.org/10.1002/pi.4455

Kazmierczak-Razna J, Nowicki P, Pietrzak R (2017) Characterization and application of bio-activated carbons prepared by direct activation of hay with the use of microwave radiation. Powder Technol 319:302-312. https://doi.org/10.1016/j.powtec.2017.06.062

Ke J, Yang K, Bai XP, Luo H, Ji YB, Chen JQ (2021) A novel chiral polyester composite membrane: Preparation, enantioseparation of chiral drugs and molecular modeling evaluation. Sep Purif Technol 255:117717. https://doi.org/10.1016/j.seppur.2020.117717

Lagerwall JPF, Schutz C, Salajkova M, Noh J, Park JH, Scalia G, Bergstrom L (2014) Cellulose nanocrystal-based materials: from liquid crystal self-assembly and glass formation to multifunctional thin films. NPG Asia Mater 6:e80. https://doi.org/10.1038/am.2013.69

Lorenz B, Oelkers M, Brand C, Kriemen E, Stephan M, Sunnick E, Yueksel D, Kumar K, Werz DB, Janshoff A (2012) Weak carbohydrate-carbohydrate interactions measured by colloidal probe microscopy. Biophys J 102:427A-427A. https://doi.org/10.1016/j.bpj.2011.11.2333

Li G, Dai X, Min YX, Zhang LL, Han SH, Shen J, Okamoto Y (2021) Influence of surfactants on the properties of cellulose derivative-based hybrid materials as chiral stationary phases. Eur Polym J 153:110492. https://doi.org/10.1016/j.eurpolymj.2021.110492

Lin CX, Chen BQ, Liu YS, Chen YT, Liu MH, Zhu JY (2021) Carboxylated cellulose nanocrystals with chiral nematic property from cotton by dicarboxylic acid hydrolysis. Carbohyd Polym 264:118039. https://doi.org/10.1016/j.carbpol.2021.118039

Lima MMD, Borsali R (2004) Rodlike cellulose microcrystals: Structure, properties, and applications. Macromol Rapid Commun 25:771-787. https://doi.org/10.1002/marc.200300268

Lu P, Hsieh YL (2010) Preparation and properties of cellulose nanocrystals: rods, spheres, and network. Carbohydr Polym 82:329-336. https://doi.org/10.1016/j.carbpol.2010.04.073

Manda R, Pagidi S, Heo Y, Lim YJ, Kim M, Lee SH (2020) Electrically tunable photonic band gap structure in monodomain blue-phase liquid crystals. NPG Asia Mater 12:42. https://doi.org/10.1038/s41427-020-0225-8

Nascimento DM, Nunes YL, Figueiredo MCB, De Azeredo HMC, Aouada FA, Feitosa JPA, Rosa MF, Dufresne A (2018) Nanocellulose nanocomposite hydrogels: technological and environmental issues. Green Chem 20:2428-2448. https://doi.org/10.1039/C8GC00205C

Palaganas NB, Mangadlao JD, De Leon AC, Palaganas JO, Pangilinan KD, Lee YJ, Advincula RC (2017) 3D printing of photocurable cellulose nanocrystal composite for fabrication of complex architectures via stereolithography. ACS Appl Mater Interfaces 9:34314-34324. https://doi.org/10.1021/acsami.7b09223

Querejeta-Fernandez A, Chauve G, Methot M, Bouchard J, Kumacheva E (2014) Chiral plasmonic films formed by gold nanorods and cellulose nanocrystals. J Am Chem Soc 136:4788-4793. https://doi.org/10.1021/ja501642p

Revol JF, Godbout L, Gray DG (1998) Solid self-assembled films of cellulose with chiral nematic order and optically variable properties. J Pulp Pap Sci 24:146-149. https://doi.org/10.1007/s001070050302

Roman M, Gray DG (2005) Parabolic focal conics in self-assembled solid films of cellulose nanocrystals. Langmuir 21:5555-5561. https://doi.org/10.1021/la046797f

Roy D, Semsarilar M, Guthrie JT, Perrier S (2009) Cellulose modification by polymer grafting: a review. Chem Soc Rev 38:2046-2064. https://doi.org/10.1039/B808639G

Saito T, Nishiyama Y, Putaux JL, Vignon M, Isogai A (2006) Homogeneous suspensions of individualized microfibrils from TEMPO-catalyzed oxidation of native cellulose. Biomacromolecules 7:1687-1691. https://doi.org/10.1021/bm060154s

Sletmoen M, Gerken TA, Stokke BT, Burchell J, Brewer CF (2018) Tn and STn are members of a family of carbohydrate tumor antigens that possess carbohydrate-carbohydrate interactions. Glycobiology 28:437-442. https://doi.org/10.1093/glycob/cwy032

Sunasee R, Hemraz UD, Ckless K (2016) Cellulose nanocrystals: a versatile nanoplatform for emerging biomedical applications. Expert Opin Drug Deliv 13:1243-1256. https://doi.org/10.1080/17425247.2016.1182491

Suresha KM, Yang SY, Lee MH, Kim JH, Kim J (2008) Actuator, sensor and MEMS devices based on regenerated cellulose. Compos Interfaces 15:679-685. https://doi.org/10.1163/156855408786778393

Tan HK, Lim RJJ, Seng HL, Shanmugam J, Ko HYY, Cheng XM, Putra V, Xing ZX, Soumyanarayanan A, Ho P (2021) Intermixing induced anisotropy variations in CoB-based chiral multilayer films. J Phys D 54:354003. https://doi.org/10.1088/1361-6463/ac09b6

Tang JT, Sisler J, Grishkewich N, Tam KC (2017) Functionalization of cellulose nanocrystals for advanced applications. J Colloid Interface Sci 494:397-409. https://doi.org/10.1016/j.jcis.2017.01.077

Wang Y.Y., Zhou ZH, Zhu JL, Sun WJ, Yan DX, Dai K, Li ZM (2021) Low-temperature carbonized carbon nanotube/cellulose aerogel for efficient microwave absorption. Compos B Eng 220:108985. https://doi.org/10.1016/j.compositesb.2021.108985

Witt H, Savic F, Oelkers M, Awan SI, Werz DB, Geil B, Janshoff A (2016) Size, kinetics, and free energy of clusters formed by ultraweak carbohydrate-carbohydrate bonds. Biophys J 110:1582-1592. https://doi.org/10.1016/j.bpj.2016.03.006

Xiong R, Singh A, Yu ST, Zhang SD, Lee H, Yingling YG, Nepal D, Bunning TJ, Tsukruk VV (2020) Co-assembling polysaccharide nanocrystals and nanofibers for robust chiral iridescent films. ACS Appl Mater Interfaces 12:35345-35353. https://doi.org/10.1021/acsami.0c08571

Zhang F, Wang D, Qin H, Feng L, Liang X, Qing G (2019) Chemoselectivity of pristine cellulose nanocrystal films driven by carbohydrate–carbohydrate interactions. ACS Appl Mater Interfaces 11:13114-13122. https://doi.org/10.1021/acsami.9b00471

Zhang XF, Xiong R, Kang SW, Yang YK, Tsukruk VV (2020) Alternating stacking of nanocrystals and nanofibers into ultrastrong chiral biocomposite laminates. Acs Nano 14:14675-14685. https://doi.org/10.1021/acsnano.0c06192

Figures

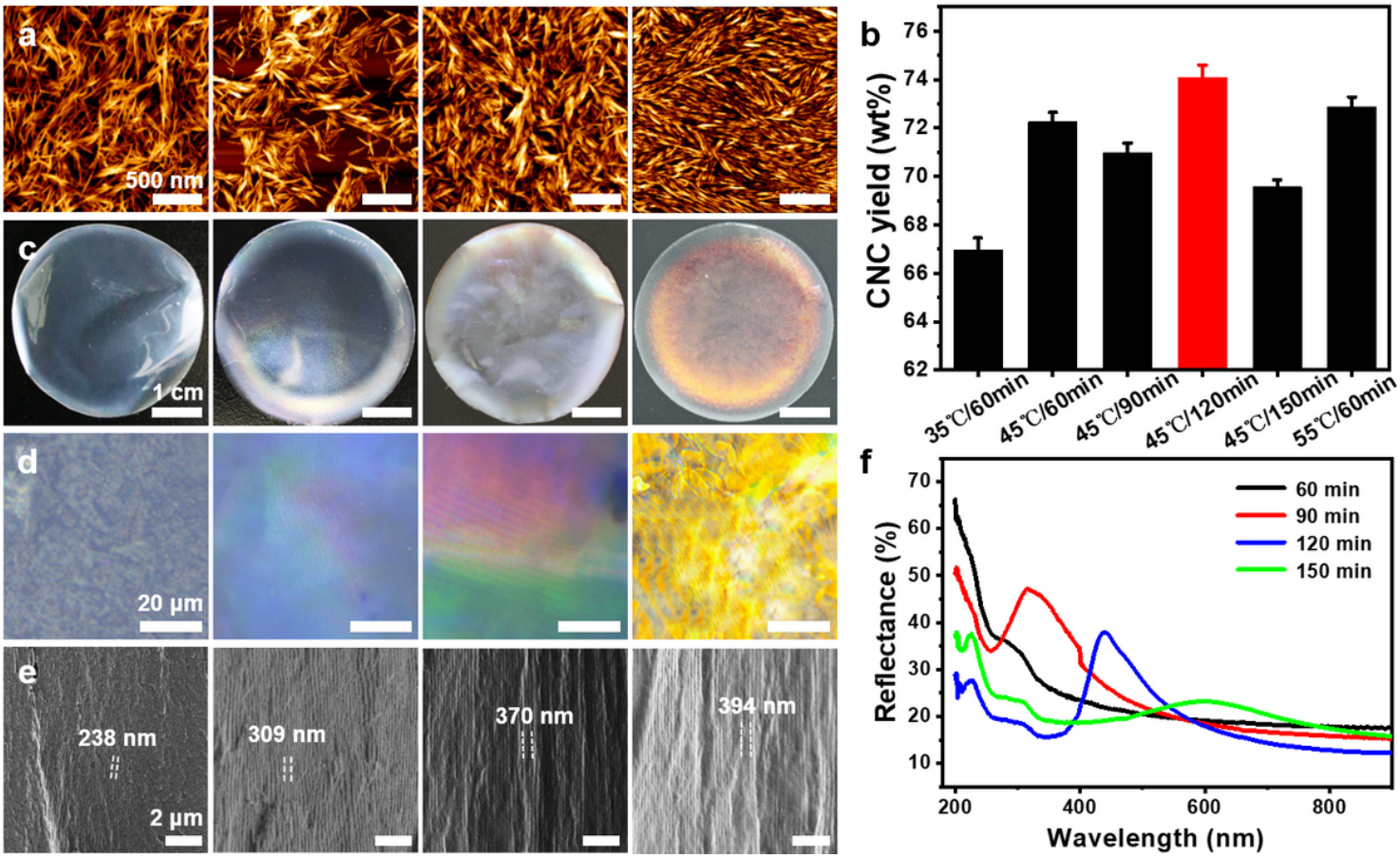

Figure 1

Characterization of pure CNC films fabricated with different hydrolysis time (from left to right: 60 mins, 90 mins, 120 mins and 150 mins). (a) AFM images of the CNC films with different hydrolysis time. (b) CNC yields under different hydrolysis time and temperatures. (c) Photographs of the films indicated different color response. (d) POM images of films with fingerprint textures; (e) SEM images of CNC films with different randomly oriented periodic pitches. (f) Reflectance spectra of films with different hydrolysis time at 45 ℃.

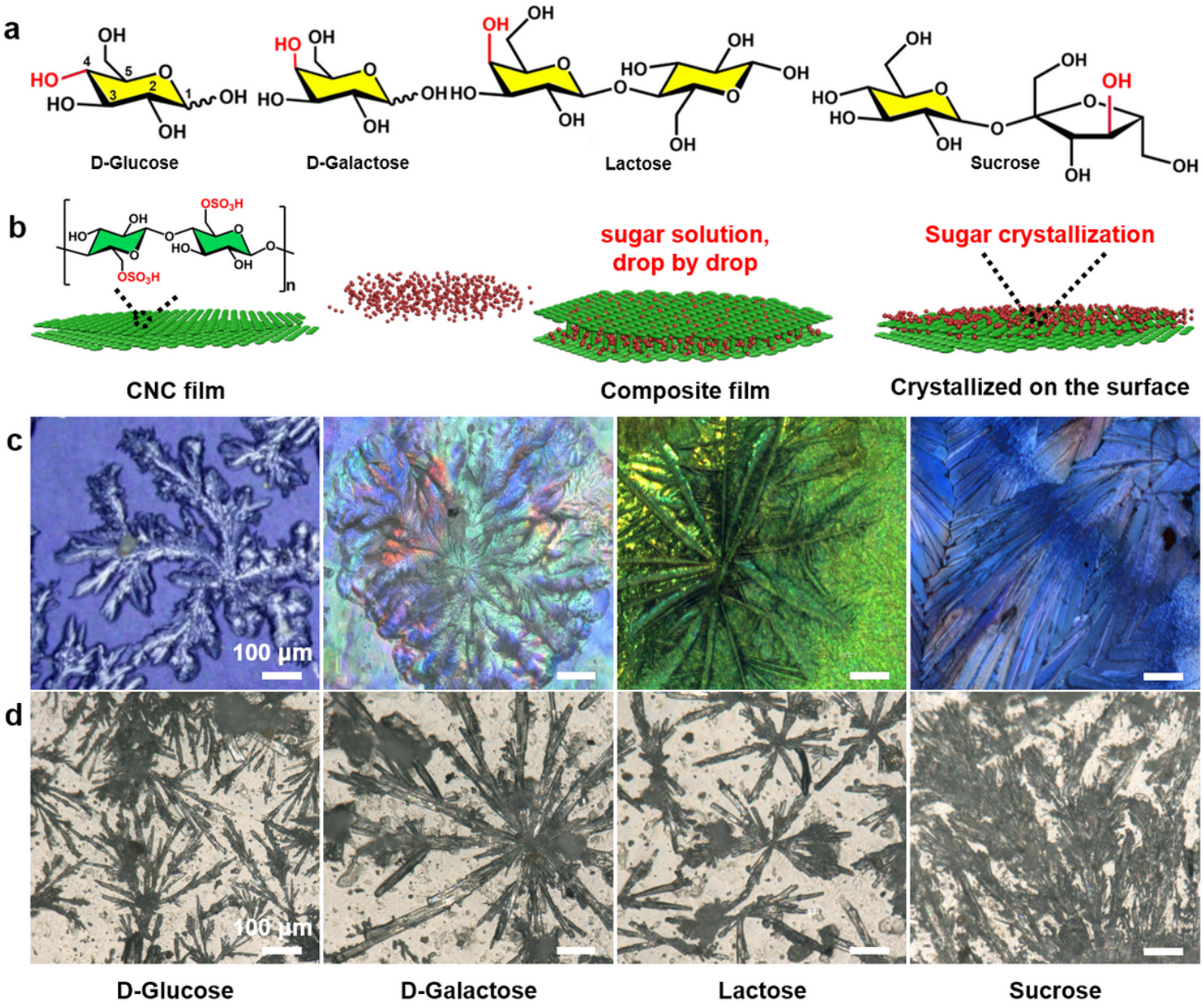

Figure 2

(a) The molecular formulas of different glucose homologs (from left to right are glucose, galactose, lactose and sucrose, respectively). (b) Schematics showing the mechanism of glucose homologs solution dripping onto the CNC film and forming crystallizations. (c) POM images showing the glucose homologs crystallization on CNC films. (d) POM images showing the glucose homologs crystallization on glass plates.

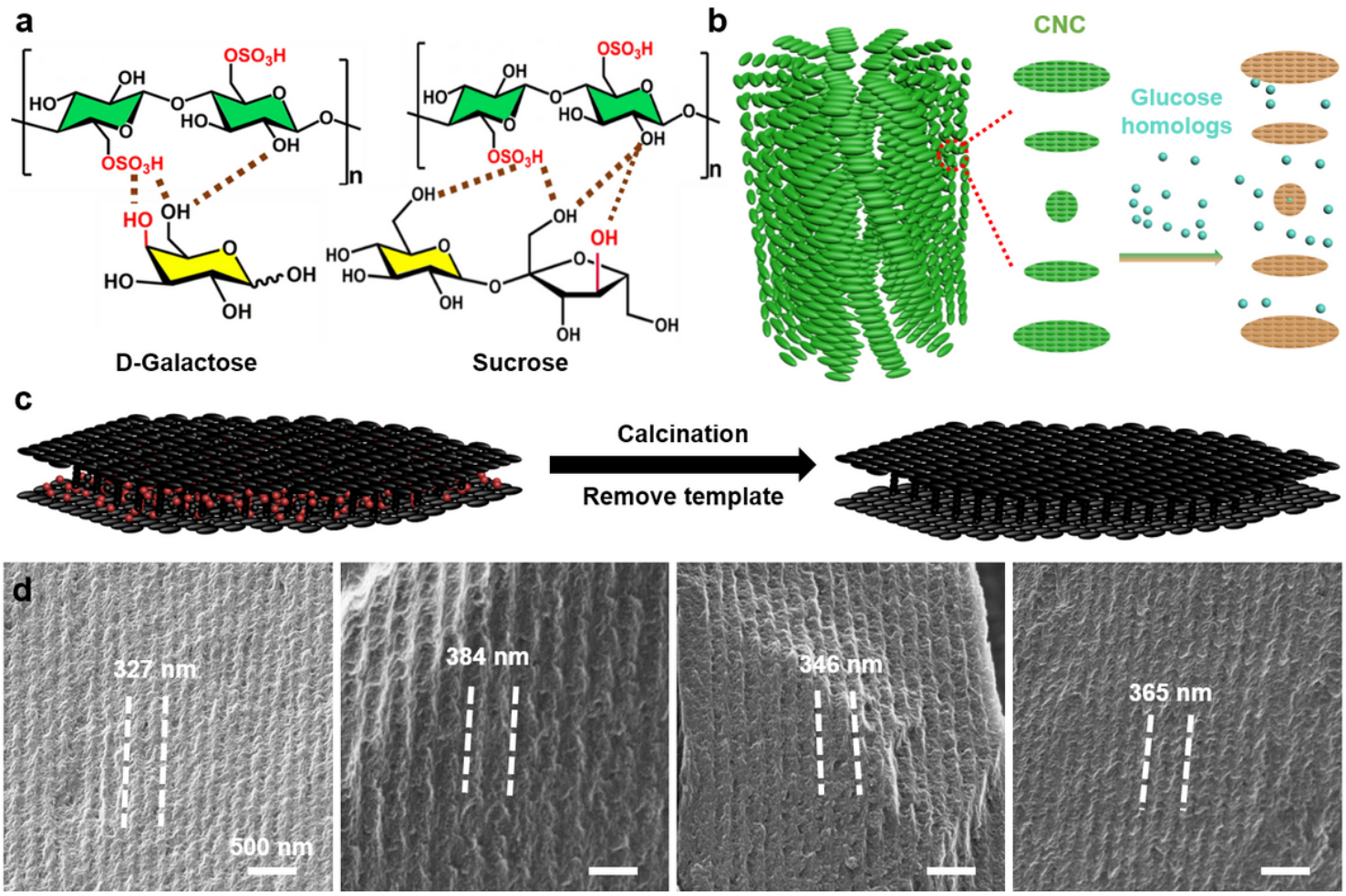

Figure 3

The process of preparing carbon film with CNCs and glucose homologs. (a) The molecular formula of CNCs and glucose homologue (d-Galactose, sucrose respectively). (b) Schematics showing the mechanism of the self-assembly process of cellulose and glucose homologs solution into a film. (c) Schematics showing the carbonization process of cellulose films. (d) SEM images of carbon films with different glucose homologs (glucose, galactose, lactose and sucrose, respectively).

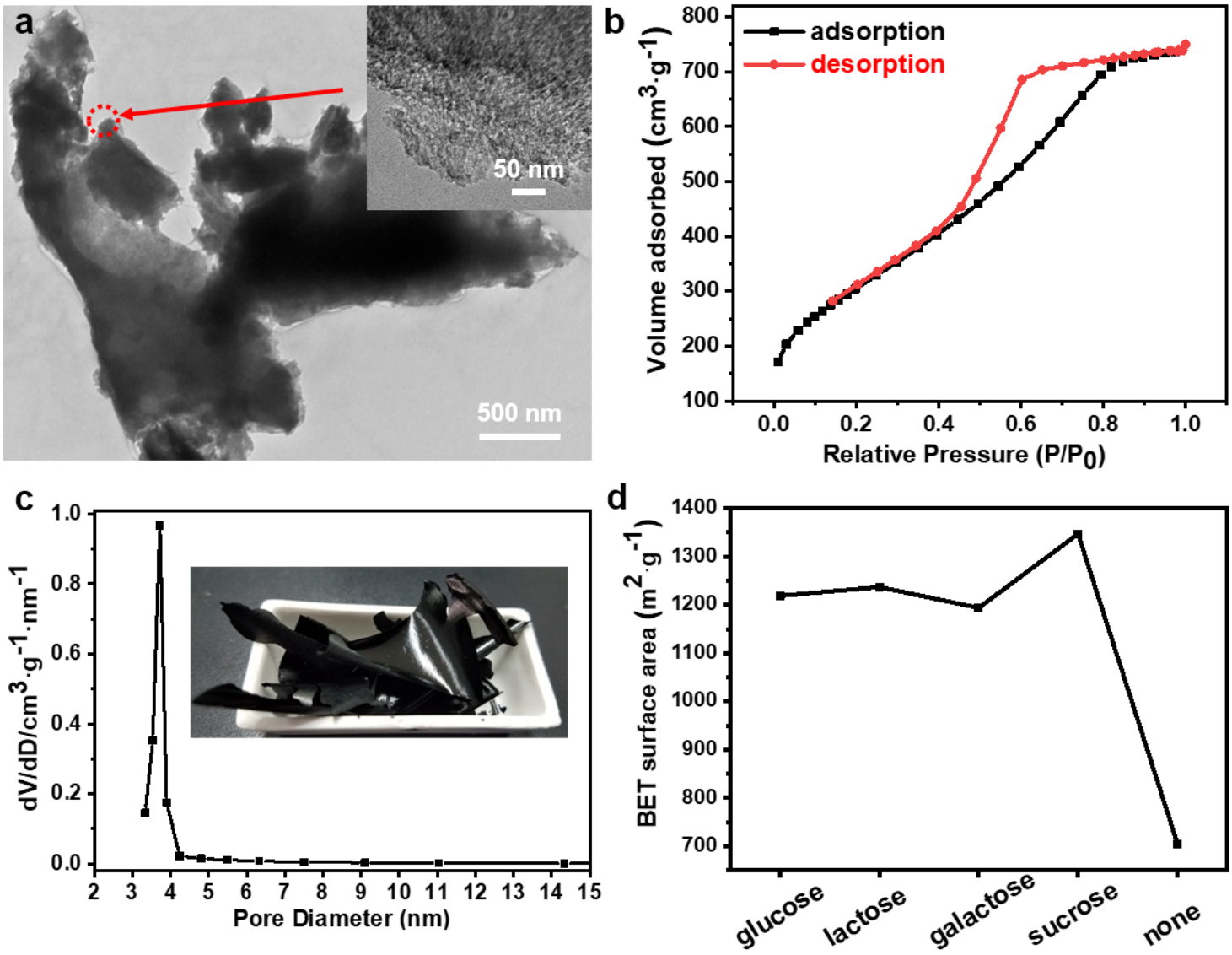

Figure 4

(a) TEM image of mesoporous carbon film with twisting rod-like morphology. (b) Nitrogen adsorption isotherms of mesoporous carbon film. (c) Photograph of a mesoporous carbon film with glossy black appearance obtained from pyrolysis and etching of the pristine CNCs/sucrose film and Barret–Joyner–Halenda pore size distribution of carbon film calculated from the adsorption branch of the nitrogen isotherms. (d) Surface areas of mesoporous carbon film with different glucose homologs based on Brunauer–Emmett–Teller (BET) theory.

Supplementary Files

This is a list of supplementary files associated with this preprint. Click to download.

- SupplementaryInformation.docx